Materials Today Communications 26 (2021) 101829

Contents lists available at ScienceDirect

Materials Today Communications

journal homepage: www.elsevier.com/locate/mtcomm

Cellulose acetate encapsulated upconversion nanoparticles – A novel theranostic platform

Seda Demirel Topel [a,*], Sevgi Balcioglu [b], Burhan Ateş [b], Meltem Asilturk [c], Önder Topel [d], Marica B. Ericson [e]

[a] Department of Electrical and Electronics Engineering, Faculty of Engineering, Antalya Bilim University, 07190 Antalya, Turkey
[b] Department of Chemistry, Faculty of Sciences, Inonu University, 44000 Malatya, Turkey
[c] Department of Material Science and Engineering, Faculty of Engineering, Akdeniz University, 07058 Antalya, Turkey
[d] Department of Chemistry, Faculty of Sciences, Akdeniz University, 07058 Antalya, Turkey
[e] Department of Chemistry and Molecular Biology, Biomedical Photonics, University of Gothenburg, 412 96 Gothenburg, Sweden

ARTICLE INFO

Keywords:
Cellulose acetate
Upconversion nanoparticles
Encapsulation
Doxorubicin
pH-triggered drug release

ABSTRACT

Luminescent upconversion nanoparticles (UCNPs) are of great interest in a wide range of nanotechnological applications, particularly in the biomedical area like imaging and therapy but their biocompatibility and stability pose major challenges hampering progression towards further pharmaceutical applications. Herein, we present a biocompatible theranostic platform enabling simultaneous diagnosis and drug delivery consisting of UCNPs encapsulated with cellulose acetate (CA), a biocompatible polymer. Luminescence properties of UCNPs in the developed theranostic platform remain stable even after encapsulation. The size of the CA capsules, ranging from micro- to nano-sized particles, can easily be tuned by adjusting the stirring rate during encapsulation. Doxorubicin, a well-known chemotherapeutic drug, onto the CA nanocapsules containing UCNPs (UCNP-CA nanocapsules) was loaded with up to ~63 % efficiency and acid-induced release (~47 %) obtained at pH 3.6 and 5.5. It was found that encapsulation decreased toxicity of UCNPs as confirmed in a cellular assay (L-929 and MCF-7 cell lines). Taken together, the developed UCNP-CA nanocapsules serve as a highly interesting novel theranostic platform, combining the biocompatible optical properties of UCNP, with reduced cell toxicity and drug encapsulating properties of CA. The proposed system could be subject for further refinement and exploration.

1. Introduction

Upconversion nanoparticles (UCNPs) are luminescent nanomaterials based on lanthanide doped rare earth nanocrystals having ability to convert a near-infrared (NIR) radiation into visible light through so called photophysical upconversion processes [1,2]. Compared to the conventional fluorescent and luminescent materials such as organic fluorophores, quantum dots and carbon dots, generally exhibiting large Stokes-shifts, UCNPs offer several advantageous optical properties like large anti-Stokes shift, high photochemical stability and sharp emission bandwidth [3]. Particularly, due to their remarkable anti-Stokes shift allowing for excitation in NIR region the UCNPs are highly interesting for medical applications such as biosensing and bioimaging potentially allowing for deep tissue imaging, high contrast potentially avoiding background autofluorescence, and reduced photodamage [4].

Targeting biomedical applications, biocompatibility and stability are two major challenges. It has been shown in earlier studies that stability of UCNPs is a problem due to their potential to agglomerate [5]. To overcome this problem, many designs have been explored modifying the surface of the UCNPs using polymers such as polyacrylic acid, polyethyleneimine, polyvinylpyrrolidone and block co-polymers or inorganic oxides such as SiO_2 and TiO_2 [6–11]. Also surface modifications using biomolecules such as DNA or RNA oligonucleotides, proteins and enzymes have been investigated [12]. So far, a few of them provided sufficient evidence to move towards translational potential [13]. Thus, there is still need for further development in order to provide UCNPs with a durable, hydrophilic and biocompatible coverage.

Nanocomposites based on self-assembly of amphiphilic polysaccharide-based copolymers have demonstrated great promise for pharmaceutical applications [14]. Particularly composites based on cellulose acetate are of high interest due to its biocompatibility, availability and biodegradability [15]. In fact, cellulose acetate is already

* Corresponding author.
E-mail address: seda.demireltopel@antalya.edu.tr (S.D. Topel).

https://doi.org/10.1016/j.mtcomm.2020.101829
Received 1 July 2020; Received in revised form 4 October 2020; Accepted 18 October 2020
Available online 4 November 2020

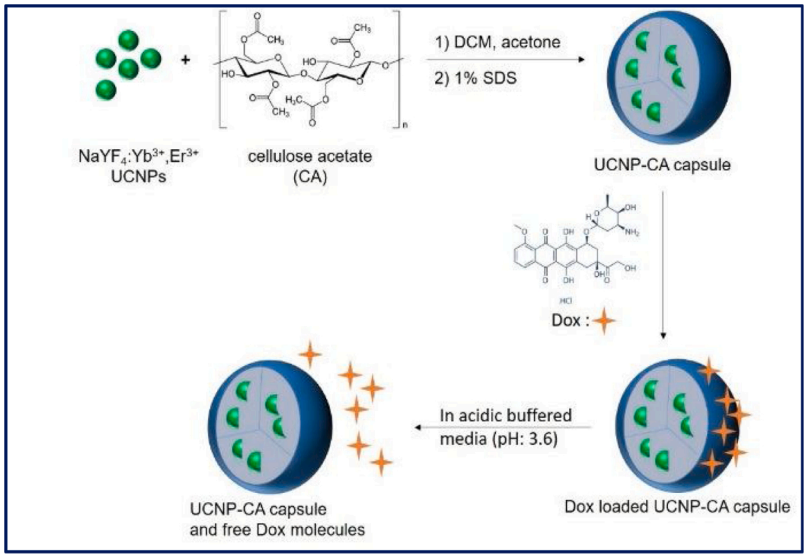

Fig. 1. Schematic illustration of the design of UCNP-CA capsule and pH responsive delivery of Dox at acidic pHs.

commercialized in several biomedical and pharmaceutical products, e.g., wound dressings, medical devices and as nanocarriers for controlled drug release [15]. In the literature, as a drug carrier platform, CA polymer is used in the form of electrospun nanofiber, core-shell nanoparticle, matrix, and microspheres in drug delivery systems [16–19]. For instance, Hujaya S. and co-workers used cellulose nanofibril (CNF), an oppositely charged polyelectrolyte, to fabricate a polyion complex hydrogel. They introduced doxorubicin (Dox) to the CNF hydrogels and investigated their pH responsive release profile. Their results showed that approximately 65 % of Dox at physiological pH 7.4 was retained past a burst release regime and the loaded Dox was completely released within 5 days at pH 4 [20]. Garg A. and co-workers prepared core-shell nanoparticles from hyaluronic acid modified cellulose acetate phthalate (HAC) and cellulose acetate phthalate (CAP) nanoparticles (NPs), and loaded an anticancer drug, 5-fluorouracil (5-FU), to the prepared nanoparticles. A significant time prolongation was observed in 5-FU release from the prepared cellulose acetate phthalate nanoparticles. 99 % of the loaded drug from 5-FU loaded CAP nanoparticles was released in 8 h, but the release time from in HAC nanoparticle system was to be found as 48 h for 97 % of the loaded drug, which indicates HAC NPs with long release time period are more effective system to deliver of 5-FU for lung cancer [21]. Wu and co-workers synthesized ibuprofen loaded-cellulose acetate (CA) composite 3D films with varying *grid void geometries* using electro-hydrodynamic printing technique. Variations in ibuprofen (IBU) release behavior was showed using minimal and identical excipients, as an example of the applications of tailored drug release, personalized medicine and tissue engineering scaffolds [22].

As mentioned above, there are several previous reports on the CA nanomaterials as a drug carrier. However, to the best of our knowledge, cellulose acetate (CA) polymers have not been investigated in context of UCNPs earlier. Herein, we present the design of a novel theranostic platform composed of the CA nanocapsules containing UCNPs (UCNP-CA nanocapsules) for the first time (Fig. 1). The UCNP-CA capsules were prepared by a solvent evaporation technique, allowing control of particle size by varying stirring rate. The optical properties of nano-sized UCNP-CA capsules were investigated using fs-pulsed NIR in a multi-photon laser scanning microscope (MPM). Furthermore, the biocompatibility and drug delivery potential were explored in a cellular assay by loading the capsules with doxorubicin (Dox), a well-known anthracycline-based chemotherapeutic drug.

2. Experimental section

2.1. Materials

Ammonium fluoride (NH_4F), Erbium(III) chloride hexahydrate ($ErCl_3.6H_2O$, 99.99 %), cerium(III) chloride hexahydrate ($CeCl_3.H_2O$, 99.99 %), sodium hydroxide (NaOH), ytterbium(III) chloride hexahydrate ($YbCl_3.6H_2O$, 99.99 %), Yttrium(III) chloride hexahydrate ($YCl_3.6H_2O$, 99.99 %), polyethyleneimine (PEI, branched polymer, MW 10.000), cellulose acetate (MW 50.000), sodium dodecyl sulphate (SDS), doxorubicin hydrochloride (Dox) and solvents (analytical grade) were used as purchased (Sigma-Aldrich) without further purification.

2.2. Synthesis of $NaYF_4$:Yb^{3+}, Er^{3+}, Ce^{3+} upconversion nanoparticles (UCNPs)

UCNPs ($NaYF_4$:Yb^{3+}, Er^{3+}, Ce^{3+}) were fabricated by hydrothermal method as described before [23]. Into a 100 mL Teflon beaker, $YCl_3.6H_2O$ (0.72 mmol, 140.59 mg), $YbCl_3.6H_2O$ (0.2 mmol, 55.58 mg), $ErCl_3.6H_2O$ (0.05 mmol, 13.68 mg), $CeCl_3.6H_2O$ (0.03 mmol, 7.39 mg) and NaCl (1 mmol, 58.44 mg) were dissolved in deionized water (4 mL). The final RE^{3+} solution after addition of 50 mL of ethanol was left for stirring for 5 min. 10 mL of 5%(w/v) aqueous PEI solution and 185.2 mg of NH_4F (5 mmol) was added to the RE^{3+} solution in the Teflon beaker. The beaker placed into the autoclave was heated at 200 °C for 3 h. The synthesized UCNPs was separated by centrifuging (8500 rpm) for 15 min and the precipitate was washed for three times with ethanol:water (1:1). The UCNPs was dried under vacuum at 40 °C [23].

2.3. Synthesis of CA capsulated UCNPs (UCNP-CA nanocapsules)

UCNPs (500 mg) and cellulose acetate (1 g) were dispersed in the mixture of DCM (60 mL) and acetone (20 mL). This mixture was added drop by drop to 300 mL of 1% (w/w) aqueous SDS solution and stirred at 10.000 rpm for 1 h at ambient temperature. At the end of the duration, the solution was added to another SDS solution (1%, 300 mL) at 1500 rpm and heated to 40 °C for 4 h. After the cooling of the final mixture down to the ambient temperature, the precipitates were collected via ultracentrifuge at 12.000 rpm. The prepared CA capsules washed for three times with deionized water (50 mL) were dried at 40 °C under vacuum (Fig. S1).

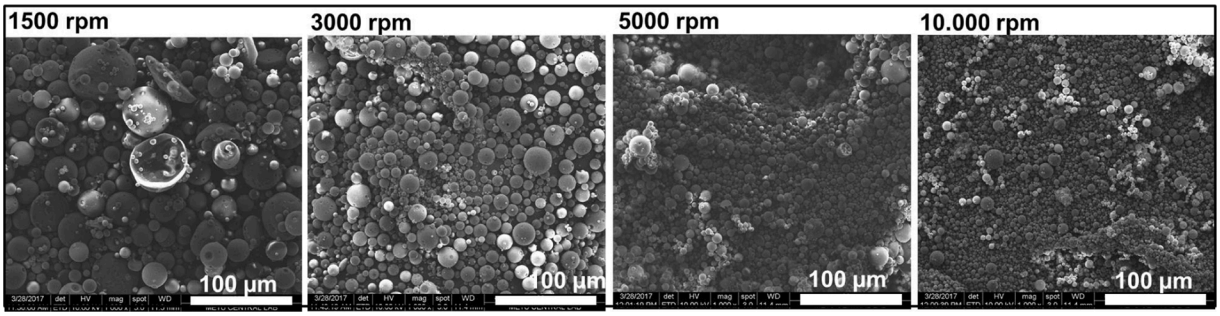

Fig. 2. SEM images of CA microcapsules formed at different stirring rates.

2.4. Characterization

The size, size distributions and surface morphology of the synthesized CA capsules, UCNPs and UCNP-CA capsules in aqueous solutions were characterized by dynamic light scattering (DLS) (Malvern Zetasizer Nano ZS), transmission electron microscopy (TEM) (LEO 906E) and scanning electron microscopy (SEM) (ZEISS) measurements. The functional groups of the synthesized particles were confirmed by FTIR spectrometer (Perkin Elmer L160000R). CA encapsulation of the UCNP-CA nanocapsules was quantified by a thermogravimetric analyzer (TGA) (Perkin Elmer, Pyris Series STA-8000) programmed with a heating rate of 10 °C/min between 30 °C and 800 °C under a nitrogen flow with 20 mL/min. Dox release was followed by a Perkin Elmer (Lambda 650) UV–vis spectrophotometer.

In photophysically characterization of imaging properties of UCNPs, a commercial upright LSM 710 NLO set up (Carl Zeiss MicroImaging GmbH, Germany) was utilized. The system was equipped with a Mai Tai DeepSee tunable NIR Ti:Sapphire fs-pulsed (< 100 fs) laser (Spectra-Physics, Newport Corporation, USA) operating at a repetition rate of 80 MHz. The excitation wavelength was set to 980 nm. The particles were places in custom made imaging chambers (Fig. S2) and imaged using a W PlanApochromat 20x/1.0 DIC M27 75 mm objective lens. Imaging conditions was kept constant for all experiments. For the power dependence measurement laser power was varied in the range 0.2–5.0 mW, as measured at the exit of objective lens. For spectral acquisition, the internal spectral detector was used with a resolution of < 10 nm. For imaging, the detected spectral range of the emission was set to 417–727 nm.

2.5. Loading of Dox to UCNP-CA nanocapsules

UCNP-CA nanocapsules (150 mg) were firstly dispersed in deionized water (20 mL) and then a Dox solution (3 mg, 1 mL deionized water) was introduced to the UCNP-CA dispersion. The mixture was left for stirring with 300 rpm for 48 h at room temperature. After this period, the mixture was dialyzed for 48 h against 500 mL of deionized water by changing outer water once every 12 h to remove unabsorbed Dox (Fig. S3). The loading level of Dox was calculated by a UV/Vis spectrometer using standard calibration curve obtained at $\lambda_{max} = 480$ nm of Dox.

2.6. In vitro drug release studies

Dox release from drug loaded UCNP-CA nanocapsules was followed by a Perkin Elmer (Lambda 650) UV–vis spectrophotometer as described before [24]. The released Dox concentration was determined according to the standard procedure by using a calibration curve created between concentrations of 5–50 ppm at 480 nm which is the maximum absorption wavelength of Dox [24].

A dialysis method was applied for *in vitro* drug release studies at pH values of 3.6, 5.5 and 7.4 by using regenerated cellulose membrane (MWCO: 3500) as explained elsewhere [24]. Firstly, Dox loaded UCNP-CA nanocapsules were divided into three equal weights. Each one was homogenously dispersed by stirring for 2 min in 2 mL phosphate buffer solutions (PBS) at pH 3.6, 5.5 and 7.4, respectively. After each dispersion was transferred into a dialysis membrane, they were immersed into three different buffer solutions (50 mL) at pH of 3.6, 5.5 and 7.4, then left for stirring at 200 rpm at room temperature. 1 mL solution taken from each vessel at certain time intervals with 2, 4, 6, 8, 24, 48, 72 h was analyzed by UV–vis spectrophotometer and then it was given back to the medium. The measurements were repeated three times and the averaged values was used to represent Dox release behavior.

Dox loading efficiency (LE%) and loading capacity (LC%) into UCNP-CA capsules were determined using Eqs. (1) and (2), respectively.

$$LE\% = \frac{W_{total\ Dox} - W_{released\ Dox}}{W_{total\ Dox}} x100 \quad (1)$$

$$LC\% = \frac{W_{total\ Dox} - W_{released\ Dox}}{W_{total\ NPs}} x100 \quad (2)$$

where $W_{total\ Dox}$ is amount (mg) of total doxorubicin in the loading solution, $W_{released\ Dox}$ is weight (mg) of doxorubicin released from dialysis membrane and $W_{total\ NPs}$ is total weight (mg) of nanoparticles.

2.7. In vitro administration in cell lines

In vitro cytotoxicity test is a significant parameter in terms of biocompatibility evaluation of the materials [25,26]. For this reason, biocompatibility of the materials was determined first with mouse fibroblast (L-929) cells and then the efficiency of the drug delivery system was investigated with breast cancer 8MCF-7) cells. Firstly, mouse fibroblast (L929) and breast cancer (MCF-7) cell lines were grown in DMEM medium with penicillin/streptomycin (1%) and FBS (10 %) in a CO_2 (5%) and air (95 %) humidified atmosphere at 37 °C. L-929 cells were used to determine the toxicity properties of UCNP, UCNP-CA and CA. The cells were seeded in 96 well-plates at 10^4 cells/well followed by exposing to UCNP, UCNP-CA and CA for 24 h with the concentrations of 12.5, 25, 50, 100 and 200 µg/mL. After the cells were washed with PBS, 10 µL of MTT (5 mg/mL in PBS) and 90 µL of DMEM were pipetted to the wells. After incubation period with 4 h at dark, the excess of MTT was removed, and 100 µL of DMSO was added. The color intensity at 550 nm was determined by a microplate reader, and the control wells were accepted as viable.

In order to determine pH-dependent toxicity of UCNP-CA capsules containing Dox against MCF-7 cells, the particles (0.1 g) were added to the DMEM medium prepared at different pH (3.6, 5.5 and 7.4) and incubated for 24 h. The medium was removed and added to the wells containing 10^4 cells per well. After 24 h incubation, the medium was separated and 10 µL of MTT (5 mg/mL in PBS) and DMEM (90 µL) were added to the wells. MTT measurements were carried out like mentioned above. Standard deviation values were given as SD.

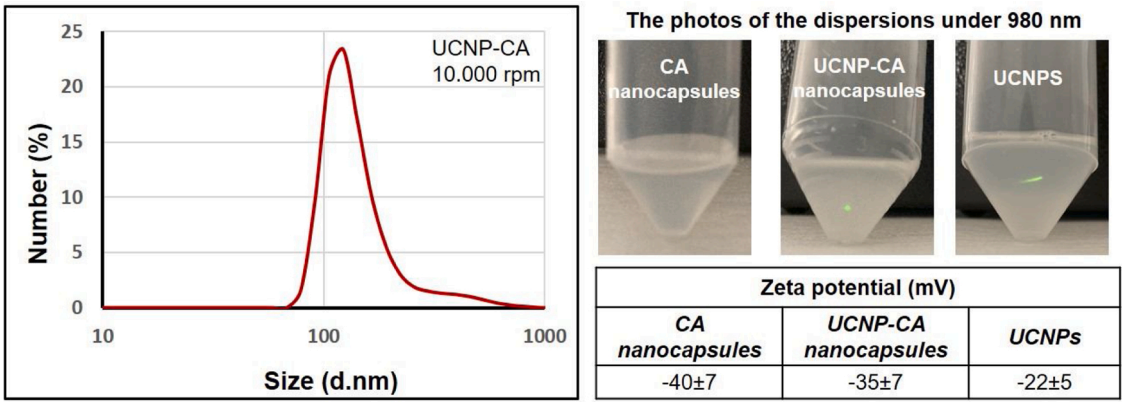

Zeta potential (mV)		
CA nanocapsules	*UCNP-CA nanocapsules*	*UCNPs*
-40±7	-35±7	-22±5

Fig. 3. DLS measurement of the UCNP-CA nanocapsules prepared at 10.000 rpm; Photo of the dispersed bare CA nanocapsules, bare UCNPs and UCNP-CA nanocapsules in PBS solution at pH:7.4; and zeta potentials of those solutions.

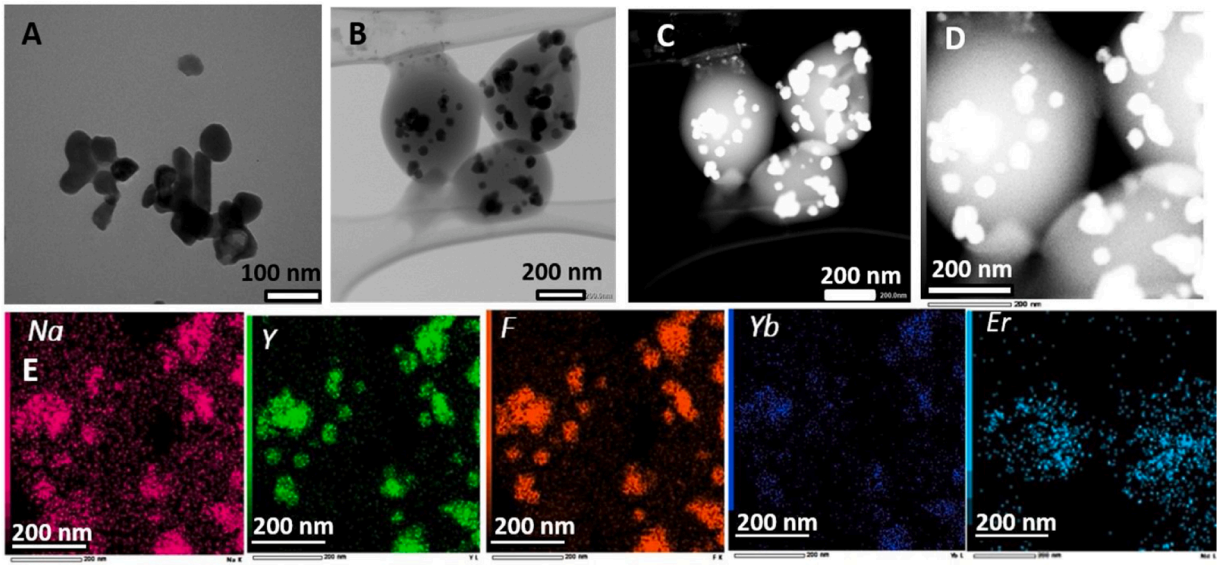

Fig. 4. (A) TEM images of bare-UCNPs, (B) UCNP-CA, (C) High angle annular dark field (HAAF) TEM image of UCNP-CA, (D) Bright field TEM image of UCNP-CA, (E) TEM mapping analysis of UCNP-CA.

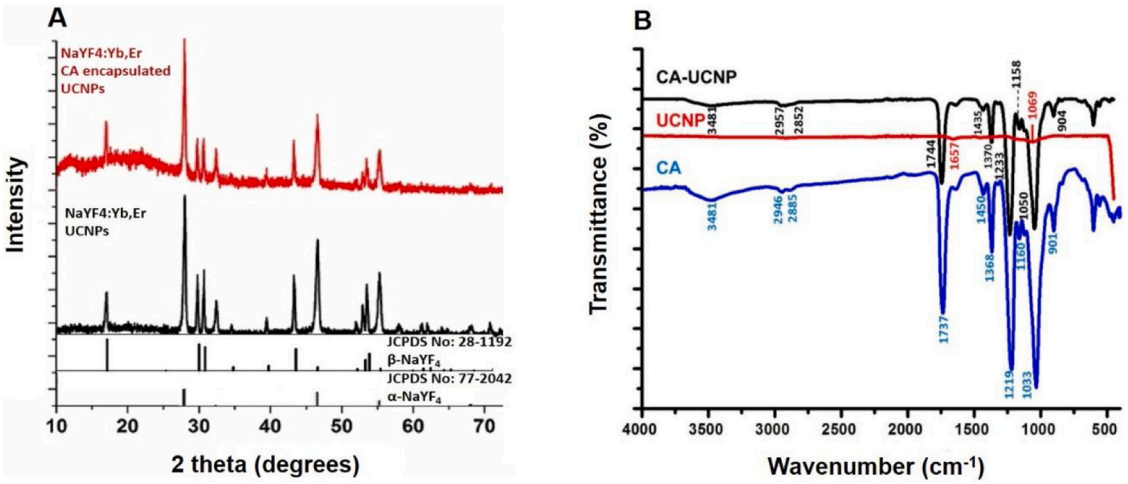

Fig. 5. (A) XRD of bare UCNP, UCNP-CA and reference XRD data, (B) FTIR spectra of bare CA microcapsules, bare UCNP and UCNP-CA.

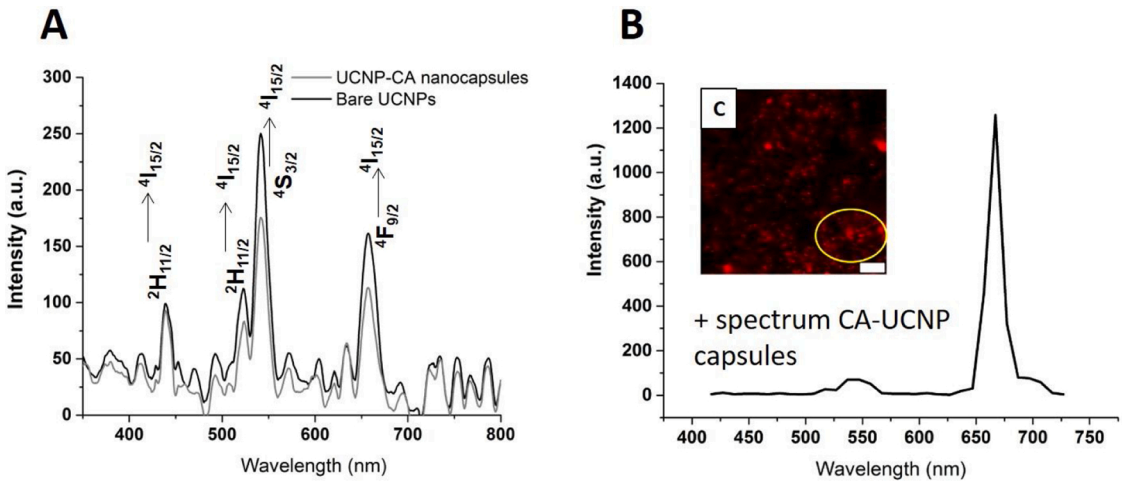

Fig. 6. (A) The comparison of luminescence emission of bare UCNPs and UCNP-CA nanocapsules dispersed in liquid medium; (B) emission spectra of CA encapsulated UCNPs ($NaYF_4$:Yb^{3+}, Er^{3+}) at room temperature acquired using pulsed (~100 fs, 80 MHz) laser operating at 980 nm. Insert in (C) shows the MPM image (400 × 400 μm) of bare UCNPs, with region of interest from which spectrum was obtained. The scale bar is 20 μm.

3. Results and discussion

3.1. Size control of CA capsules

The size of CA capsules is an important parameter that should be optimized with respect to cellular uptake and biodistribution [27]. Therefore, first, bare CA capsules were prepared by controlling the stirring rate. Four different stirring rates (1500, 3000, 5000, and 10.000 rpm) were studied, and the SEM images showed that as the stirring rate was increased, the size of capsules was significantly decreased (Fig. 2). As a result, at 10.000 rpm, the average size of the CA capsules was determined as 320 ± 5 nm which is proper for the biological studies. After the stirring rate for suitable CA capsule size was optimized, the pre-synthesized UCNPs were then employed to encapsulate within CA nanocapsules in situ at 10.000 rpm.

3.2. Encapsulation and characterization of UCNP-CA nanocapsules

The aim was to create a biocompatible theranostic platform based on CA encapsulated UCNPs and, to improve water dispersibility of the UCNPs. Bare UCNPs generally tend to be agglomerate in aqueous solutions. As a result of encapsulation with CA of the particles, the stability of UCNPs in water increased and they stayed over a week without any precipitation in PBS buffer solution at pH 7.4 (Fig. 3). Zeta potential measurements of bare UCNPs, bare CA and UCNP-CA dispersions was also confirmed the stability. Furthermore, the zeta potential of the bare UCNPs −22 ± 7 mV has been increased to –35 ± 7 mV after encapsulation with CA which proves the UCNP-CA nanocapsules are stable in the aqueous solution (Fig. 3).

To prove the encapsulation of UCNPs into CA nanocapsules, UCNP-CA nanocapsules were visualized by TEM measurements, as seen in Fig. 4. TEM measurements were also applied to determine size, size distribution and morphology of the pre-synthesized UCNPs. It was found the UCNPs to have both spherical shape with the diameter of 50 ± 2 nm and rod shape with the width of 25 ± 1 nm, and the length of 80 ± 5 nm, respectively (Fig. 4A). Fig. 4B clearly shows that UCNPs have been successfully imprisoned in the CA nanocapsules. The nanoparticles with dark colour represent the UCNPs, while the lighter spheres representing CA nanocapsules (Fig. 4B).

Fig. 4C and D demonstrate dark and bright field TEM images of the CA encapsulated UCNPs, respectively. In order to prove the lanthanide (III) ions doping to $NaYF_4$ nanocrystals, elemental mapping in STEM image showing UCNP-CA nanocapsules was performed and the results showed that Yb^{3+} and Er^{3+} ions were successfully doped into the host crystal lattice (Fig. 4E). Crystal phase of UCNPs was further characterized by XRD measurements (Fig. 5A). The peaks indexed to the planes belonging hexagonal phase (β–$NaYF_4$) and the cubic (α–$NaYF_4$) in XRD pattern are in good agreement with the reference JCPDS 28–1192 and JCPDS 77–2042, respectively [28]. The synthesized UCNPs are therefore a mixture of hexagonal and cubic phases. It is favorable the presence of hexagonal phases of $NaYF_4$ nanocrystals in the media since the upconversion efficiency of hexagonally crystalized lanthanide doped $NaYF_4$ nanocrystals is higher than that of the cubic phase [29].

To further prove the CA encapsulation, FTIR spectra of bare CA microcapsules, bare UCNPs and CA encapsulated UCNPs nanocapsules are exhibited in Fig. 5B. The FTIR spectrum of cellulose acetate microcapsules showed characteristic bonds belonging ester functional group at 1737 cm^{-1} (CO═ stretching), 1450 cm^{-1} (aliphatic CH— in-plane bending for CH_3—CO), 1368 cm^{-1} (CH_3 symmetric deformation), 1219 cm^{-1} (C—OC— asymmetric stretching), 1160 cm^{-1} (C—OC— symmetric stretching). The hydroxyl group of *D*-glycose unit in CA was appeared at 3481 cm^{-1} as a broad band and the vibrations of the aliphatic CH— strength of *D*-glycose was seen at 2946 and 2885 cm^{-1}. The asymmetric and symmetric stretching modes of C—OC— bond were appeared at 1033 cm^{-1} and 901 cm^{-1}, respectively [30]. After encapsulation of the UCNP by CA, the vibrations of the functional groups of CA were shifted to higher wavenumber and the peaks belong to UCNP-CA nanocapsules were appeared at 1744 cm^{-1} for CO═ stretching, 1370 cm^{-1} for CH_3 symmetric deformation, 1233 cm^{-1} for CO— stretching and 1050 cm^{-1} for C—OC— stretching.

In order to quantify the amount of CA in the UCNP-CA capsules, thermal gravimetric analysis (TGA) measurements have been performed (Fig. S4). TGA curve of bare CA capsules showed 87.1 % weight loss due to the decomposition of the organic polymer, CA [31]. It was also observed 12.9 % residual after CA decomposition. On the other hand, UCNP-CA capsules lost 54.5 % weight due to the burning of CA polymer. The rest of 45.5 % sum of UCNPs and the residual of CA. According to the TGA curve of bare CA capsules, it was estimated that the UCNP-CA capsules constitutes 38.6 % of UCNPs.

3.3. Photophysical characterization

The upconversion phenomena occurs a result of multi-step absorption from resonant states in lanthanide ions having metastable *4f-4f* intermediate states after the excitation of the nanoparticle with low energy photons in the near-infrared (NIR) region, [32,33], and are generally known as the conversion of NIR light to UV and visible regions. Generally, a sensitizer ion such as Yb^{3+} having a stronger absorption

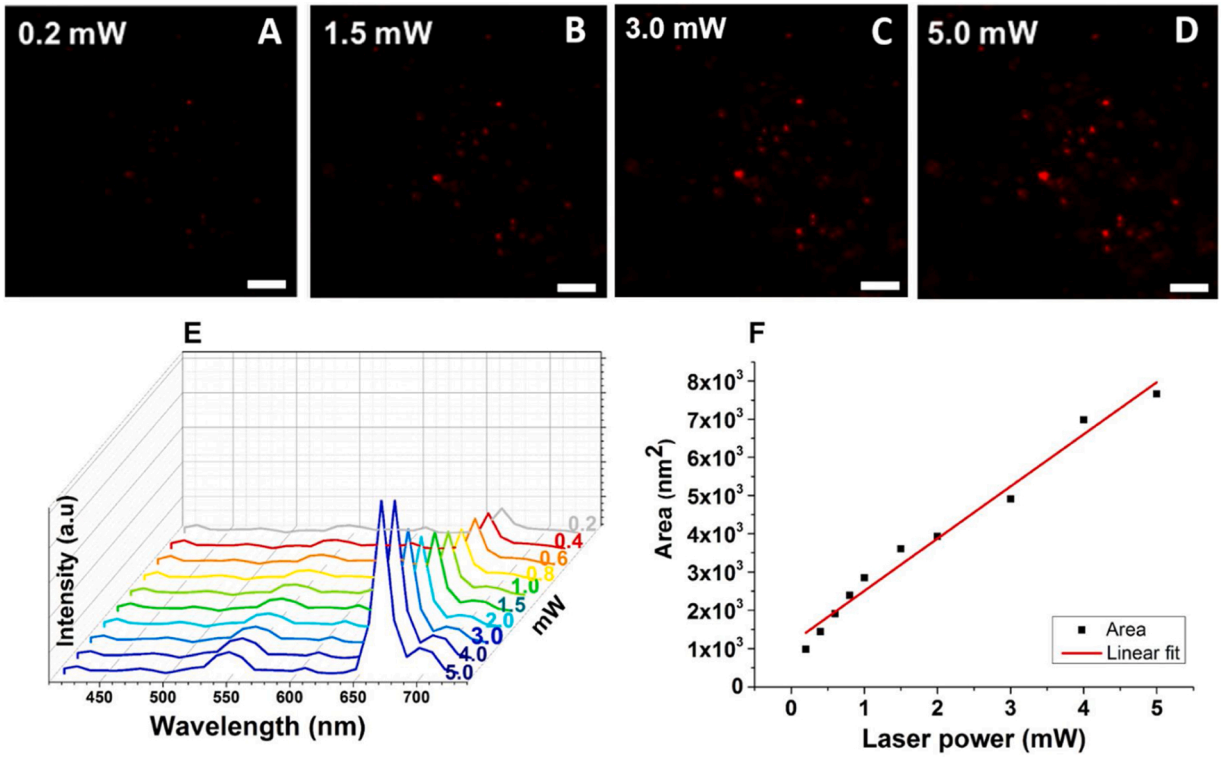

Fig. 7. CA encapsulated UCNPs ($NaYF_4$:Yb^{3+}, Er^{3+}) visualized by MPM operating at ambient room temperature using 980 nm excitation from a fs-pulsed (~100 fs, 80 MHz) laser. (A-D) MPM images (400 × 400 μm) acquired at different average laser powers (0.2-5.0 mW), (E) emission spectrum from particles using different laser powers, and (F) the correlation between I_{UCPL} as function of P together with a linear fit. The scale bar is 20 μm.

ability in the NIR region and an emitter ion/ions such as Er^{3+}, Tm^{3+} or Ho^{3+} ions having a resonance energy level with the sensitizer ion is required [33,34]. Fig. 6A illustrates the emission of $NaYF_4$:Yb, Er UCNPs appeared at 439, 523, 541 and 659 nm corresponding to $^2H_{9/2} \rightarrow {}^4I_{15/2}$, $^2H_{11/2} \rightarrow {}^4I_{15/2}$, $^4S_{3/2} \rightarrow {}^4I_{15/2}$ and $^4F_{9/2} \rightarrow {}^4I_{15/2}$ transitions, respectively, measured with a fluorescence spectrophotometer in a liquid media. After encapsulation with CA, the luminescence emission intensity of UCNPs has been decreased 30 % observed at the characteristic emission peaks of Erbium. The narrow emission bands at 550 and 670 nm, belonging the characteristic *4f–4f* transitions of Er^{3+} doped UCNPs appear in both the bare as well as in the CA encapsulated particles, confirming that optical properties are retained after encapsulation. Included in the Fig. 6B is the spectra acquired using pulsed laser (~100 fs, 80 MHz) in a multiphoton microscope (MPM). The rationale for this comparison was to confirm the relevance of the theranostic system also for applications based on MPM.

Since the principle of MPM is based on the inherent confocal properties of multiphoton processes, it is interesting to study how the UCNPs excitation behaves in the MPM at varying laser power. It has been reported that the intensity of UC photoluminescence (I_{UCPL}) has a non-linear dependence on power of excitation light (P), *i.e.*, $I_{UCPL} = kP^n$, where n is the number of photons required to generate the UC luminescence [32]; however, it is also stated that the values of "n" can be reduced by completion of decay and upconversion rates. Thus, in this study the particles where excited at different laser powers using MPM and pulsed NIR light, as demonstrated in Fig. 7. Evident from the Fig. 7F is a linear power dependence observed, implying that the excitation of UCNPs in the MPM is not following a non-linear dependence.

3.4. *In vitro pH triggered Dox release*

Doxorubicin (Dox), being a well-known anthracycline-based chemotherapeutic drug, has in recent years been explored in combination with various nano-systems in order to increase its targeting via active or passive targeting process, and also to overcome the disadvantages of unspecific cell toxicity associated with chemotherapeutic drugs [35]. Such nano-systems can control the release of a chemotherapeutic drug to the targeted area with stimulants such as pH, temperature, glutathione, redox potential, magnetic field, ultrasound, or light [36,37]. Among these triggers, pH is an important parameter in targeted drug delivery systems, because the extracellular pH of the tumor tissues between 5.8–7.4 is lower than that of blood plasma and healthy tissues (pH 7.4). In particular, pH in the intracellular parts such as endosomes (pH 5–6) and lysosomes (pH 4–5) further drops further till 4–5 [38]. Hence, many drug carrier systems have been designed as pH sensitive drug delivery systems.

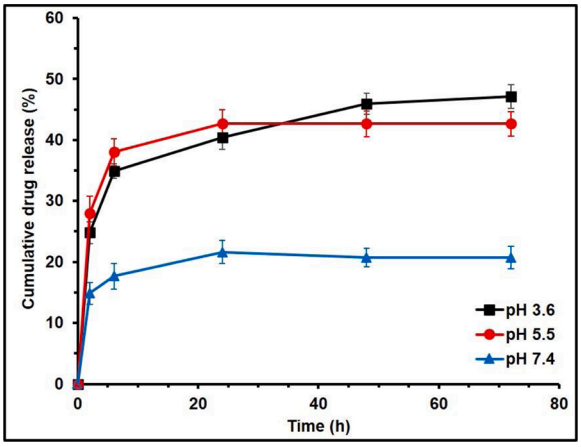

Fig. 8. Drug release profiles of UCNP-CA nanocapsules at pH 3.6, 5.5 and 7.4.

In the present study, we designed our system according to pH depended drug release from UCNP-CA nanocapsules. It has been chosen

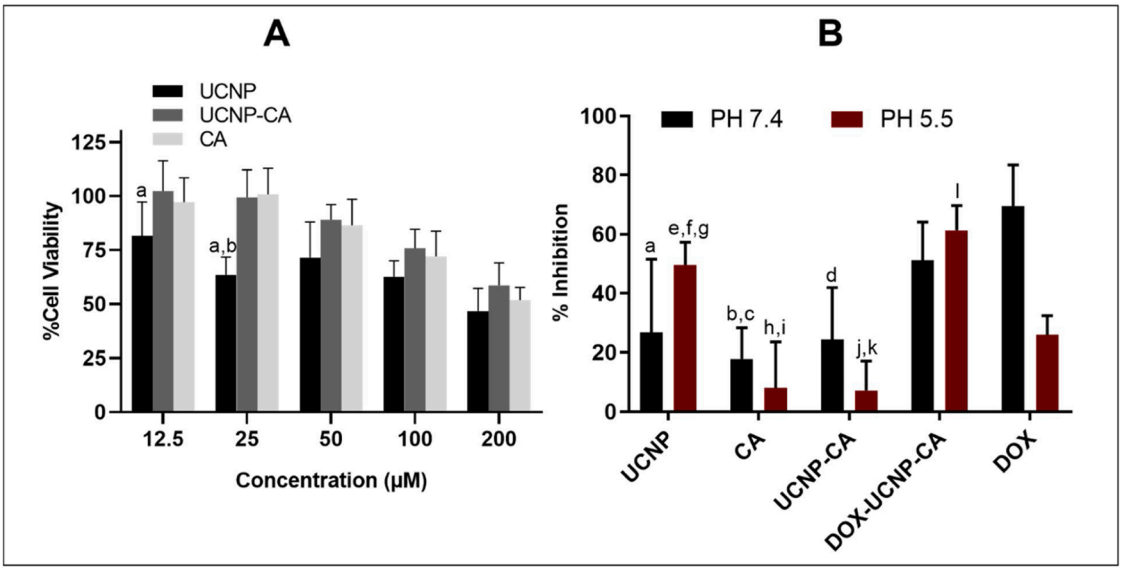

Fig. 9. (A) MTT assay of the viability of L929 cells after treatment with different concentrations of UCNP, UCNP-CA and CA of UCNP, UCNP-CA and CA for 24 h. Statistically significant values ($p < 0.05$); a: UCNP vs UCNP-CA, b: UCNP vs CA. (B) % inhibition results of UCNP, CA, UCNP-CA, Dox-UCNP-CA and Dox against MCF-7 cells under different pHs. Statistically significant values ($p < 0.05$); pH 7.4; a: UCNP vs Dox, b: CA vs Dox-UCNP-CA, c: CA vs Dox, d: UCNP-CA vs Dox, pH 5.5; e: UCNP vs CA, f: UCNP vs UCNP-CA, g: UCNP vs Dox, h: CA vs Dox-UCNP-CA, i: CA vs Dox, j: UCNP-CA vs Dox-UCNP-CA, k: UCNP-CA, l: Dox-UCNP-CA vs Dox.

a well-known chemotherapy drug, doxorubicin (Dox) which is an anthracycline-based chemotherapy drug for a variety of cancer therapy, including breast cancer, melanoma, lung cancer, glioma, leukaemia and lymphoma [39] since Dox molecules can easily be adsorbed to the surface of CA capsules via weak electrostatic forces. At acidic pH conditions, Dox is protonated and become quite water-soluble, thus it release from the CA surface to the medium. The release profiles of Dox loaded onto the UCNP-CA capsules were monitored by UV–vis spectrophotometer. The results show that the Dox molecules were adsorbed onto the UCNP-CA nanocapsules with 63 % of loading efficiency and 1.1 % of loading capacity. Then, *in vitro* drug release from Dox loaded UCNP-CA nanocapsules was carried out at different pH values as depicted in Fig. S3. Fig. 8 shows drug release profiles of the UCNP-CA nanocapsules at pH 3.6, 5.5 and 7.4. At physiological pH 7.4, 21 % of Dox from UCNP-CA capsules was released at the end of 72 h while the release increased to 43 % and 47 % at pH 5.5 and 3.6, respectively. The Dox release in the capsules at pH 5.5 and 7.4 was reached to equilibrium within 20 h and the cumulative release at the equilibrium is 43 % and 21, respectively. However, 89 and 86 % of the equilibrium values were reached within 6 h respectively. On the other hand, any equilibrium at pH 3.6 has not been established for drug release even after 72 h. In fact, 75 % of the maximum value for 72 h was released at the end of 6 h at pH 3.6. Therefore, in terms of kinetics, Dox release from drug loaded UCNP-CA capsules at pH 5.5 and 7.4 was faster and the release reached to equilibrium within 20 h. On the other hand, the Dox release rate was slower at pH 3.6, but the release continued even after 72 h.

The bare UCNPs were found to be slightly toxic towards mouse fibroblast (L929) and breast cancer (MCF-7) cell lines (Fig. 9A and B). Interestingly, the toxicity of UCNPs was reduced via encapsulating with CA. According to the MTT results in Fig. 9A, bare UCNPs showed toxicity at all concentrations against L-929 cells, which agrees with the reported studies [40], however their toxicity was significantly reduced by CA encapsulation ($p < 0.05$). On the other hand, drug release efficiency study with MCF-7 showed a low toxicity value in UCNP-CA capsules, especially at pH 5.5, whereas Dox adsorbed UCNP-CA capsules showed higher inhibition compared to free Dox, indicating that drug release was achieved under acidic conditions and the anticancer drug Dox was adsorbed to UCNP-CA nanoparticles successfully (Fig. 9B). These results are correlated with the "*in vitro* pH-triggered Dox release" studies. Higher release of Dox at lower pH is also correlated with the literature [41]. In Fig. S5, pH-dependent toxicity images of MCF-7 showed that pH 3.6 caused cell damage whereas pH 5.5 and 7.4 does not exhibit such a damage. Therefore, only pH 5.5 and 7.4 results are given in Fig. 9B. In the view of the results, it is clearly seen that CA coating decreases the cytotoxicity of UCNPs, but the targeting molecules have acceptable toxicity on L-929 cells. In summary, encapsulation with cellulose acetate (CA) of UCNPs has an important role in the decreasing of cytotoxicity of UCNP and therefore the fabricated UCNP-CA nanocapsules are promising for use as a drug carrier capable of pH dependent Dox release.

4. Conclusion

As a conclusion, an efficient theranostic platform based on cellulose acetate (CA) encapsulated UCNPs have been developed and their photophysical properties, cytotoxicity, biocompatibility, and pH triggered Dox release property *in vitro* have been investigated. The encapsulation of the CA not only was diminished the toxicity of UCNPs but also increased the biocompatibility of the UCNPs towards to L929 cells. A chemotropic drug, doxorubicin, can be loaded on the designed UCNP-CA nanocapsules with 63 % of loading efficiency, successfully. The Dox loaded UCNP-CA nanocapsules showed better *in vitro* Dox release behavior at low pHs which is promising for tumor tissues since their cellular microenvironment is more acidic. Cellular experiments on MCF-7 cells shows the cells to be damaged at pH 3.6, whereas pH 5.5 and 7.4 does not exhibit such damage. In the light of the results outlined above and the efficient luminescence properties of UCNPs, the developed UCNP-CA nanocapsules have a great potential as a novel theranostic platform for bio-imaging and stimulant responsive drug release carriers.

Declaration of Competing Interest

The authors report no declarations of interest.

Acknowledgements

The Scientific Research Projects Coordination Unit of Akdeniz University (project no. FBA–2016–1808) and Swedish Research Council (VR 2015–05002) are gratefully acknowledged for the financial support.

Appendix A. Supplementary data

Supplementary material related to this article can be found, in the online version, at doi:https://doi.org/10.1016/j.mtcomm.2020.101829.

References

[1] M. Haase, H. Schäfer, Upconversion nanoparticles, Angew. Int. Chem. Ed. 50 (2011) 5808–5829.
[2] S. Wen, J. Zhou, K. Zheng, A. Bednarkiewicz, X. Liu, D. Jin, Advances in highly doped upconversion nanoparticles, Nature Commun. 9 (2018) 1–12.
[3] G. Tessitore, G.A. Mandl, M.G. Brik, W. Park, J.A. Capabianco, Recent insights into upconverting nanoparticles: spectroscopy, modeling, and routes to improved luminescence, Nanoscale 11 (2019) 12015–12029.
[4] X. Wu, G. Chen, J. Shen, Z. Li, Y. Zhang, G. Han, Upconversion nanoparticles: a versatile solution to multiscale biological imaging, Bioconjugate Chem. 26 (2015) 166–175.
[5] A. Gee, X. Xiaoxue, Surface functionalisation of upconversion nanoparticles with different moieties for biomedical applications, Surfaces 1 (2018) 96–121.
[6] X. Jia, J. Yin, D. He, K. Wang, M. Chen, Y. Li, Polyacrylic acid modified upconversion nanoparticles for simultaneous pH-triggered drug delivery and release imaging, J. Biomed. Nanotechnol. 9 (2013) 2063–2072.
[7] A.E. Guller, A. Nadort, A.N. Generalova, E.V. Khaydukov, A.V. Nechaev, I. A. Kornienko, E.V. Petersen, L. Liang, A.B. Shekhter, Y. Qian, E.M. Goldys, A. V. Zvyagin, Surface design of upconversion nanoparticles withpolyethylenimine coating for biomedical applications: better safethan brighter? ACS Biomater. Sci. Eng. 4 (2018) 3143–3153.
[8] N.J.J. Johnson, N.M. Sangeetha, J.C. Boyer, F.C.J.M. Van Veggel, Facile ligand-exchange with polyvinylpyrrolidone and subsequent silica coating of hydrophobic upconverting β-NaYF4:Yb3+/Er3+nanoparticles, Nanoscale 2 (2010) 771–777.
[9] Y.C. Chung, C.H. Yang, R.H. Lee, T.L. Wang, Dual stimuli-responsive block copolymers for controlled release triggered by upconversion luminescence or temperature variation, ACS Omega 4 (2019) 3322–3328.
[10] J.N. Liu, W.B. Bu, J.L. Shi, Silica coated upconversion nanoparticles: a versatile platform for the development of efficient theranostics, Acc. Chem. Res. 48 (2015) 1797–1805.
[11] S. Demirel Topel, Ö. Topel, G. Turgut Cin, Fabrication and characterization of TiO2 nanoparticles conjugated luminescence upconversion nanoparticles, Biointerface Res. Appl. Chem. 3 (2018) 3197–3202.
[12] A. Sedlmeier, H.H. Gorris, Surface modification and characterization of photon-upconverting nanoparticles for bioanalytical applications, Chem. Soc. Rev. 44 (2015) 1526–1560.
[13] S. Liu, W. Li, S. Gai, G. Yang, C. Zhong, Y. Dai, F. He, P. Yang, Y.D. Suh, A smart tumor microenvironment responsive nanoplatform based on upconversion nanoparticles for efficient multimodal imaging guided therapy, Biomater. Sci. 7 (2019) 951–962.
[14] P. Kothamasu, H. Kanumur, N. Ravur, C. Maddu, R. Parasuramrajam, S. Thangavel, Nanocapsules: the weapons for novel drug delivery systems, Bioimpacts 2 (2012) 71–81.
[15] M. Jorfi, E.J. Foster, Recent advances in nanocellulose for biomedical applications, J. Appl. Polym. Sci. 132 (2015) 41719–41737.
[16] K. Khoshnevisan, H. Maleki, H. Samadian, S. Shahsavari, M.H. Sarrafzadeh, B. Larijani, F.A. Dorkoosh, V. Haghpanah, M.R. Khorramizadeh, Cellulose acetate electrospun nanofibers for drug delivery systems: applications and recent advances, Carb. Polym. 198 (2018) 131–141.
[17] V. Guarino, T. Caputo, P. Calcagnile, R. Altobelli, C. Demitri, L. Ambrosio, Core/shell cellulose-based microspheres for oral administration of ketoprofen lysinate, J. Biomed. Mater. Res. B. Appl. Biomater. 106 (2018) 2636–2644.
[18] S.T. Lee, J.N. Pang, Z.A. Jawad, Functionalised multi-walled carbon nanotubes/cellulose acetate butyrate mixed matrix membrane for CO2/N2 separation, J. Phys. Sci. 30 (2019) 99–135.
[19] H.Y. Zhou, X.G. Chen, C.S. Liu, X.H. Meng, L.J. Yu, X.Y. Liu, N. Liu, Chitosan/cellulose acetate microspheres preparation and ranitidine release in vitro, Pharm. Dev. Technol. 10 (2005) 219–225.
[20] S. Hujaya, G.S. Lorite, S.J. Vainio, H. Liimatainen, Polyion complex hydrogels from chemically modified cellulose nanofibrils: structure-function relationship and potential for controlled and pH-responsive release of doxorubicin, Acta Biomater. Odontol. Scand. 75 (2018) 346–357.
[21] A. Garg, G. Rai, S. Lodhi, A.P. Jain, A.K. Yadav, Hyaluronic acid embedded cellulose acetate phthlate core/shell nanoparticulate carrier of 5-fluorouracil, Int. J. Bio. Macromol. 87 (2016) 449–459.
[22] S. Wu, Z. Ahmad, J. Li, M. Chang, Controlled engineering of highly aligned fibrous dosage form matrices for controlled release, Mater. Lett. 232 (2018) 134–137.
[23] S. Demirel Topel, G. Turgut Cin, E.U. Akkaya, Near IR excitation of heavy atom free Bodipy photosensitizers through the intermediacy of upconverting nanoparticles, Chem. Commun. (Camb.) 50 (2014) 8896–8899.
[24] S. Demirel Topel, T.G. Polat, pH responsive carboxymethyl cellulose conjugated superparamagnetic iron oxide nanocarriers, J. Sci. Perspect. 3 (2019) 99–110.
[25] X. Gao, S. Li, F. Ding, H. Fan, L. Shi, L. Zhu, J. Li, J. Feng, X. Zhu, Rapid detection of exosomal microRNAs using virüs-mimicking fusogenic vesicles, Angew. Chem. Int. Ed. 58 (2019) 8719–8723.
[26] Y. Li, K.h. Yun, H. Lee, S.H. Goh, Y.G. Suh, Y. Choi, Porous platinum nanoparticles as a high-Z and oxygen generating nanoenzyme for enhanced radiotherapy in vivo, Biomaterials, 197 8 (2019) 12-19.
[27] J. Zhao, H. Lu, S. Wong, M. Lu, P. Xiao, M.H. Stenzel, Influence of nanoparticle shapes on cellular uptake of paclitaxel loaded nanoparticles in 2D and 3D cancer models, Polym. Chem. 8 (2017) 3317–3326.
[28] M. Ding, S. Yin, Y. Ni, C. Lu, D. Chen, J. Zhong, Z. Ji, Z. Xu, Controlled synthesis of β-NaYF4:Yb3+/Er3+ microstructures with morphology- and size-dependent upconversion luminescence, Ceramics Int. 41 (2015) 7411–7420.
[29] G. Yi, G.M. Chow, Synthesis of hexagonal-phase NaYF4:Yb,Er and NaYF4:Yb,Tm nanocrystals with efficient up-conversion fluorescence, Adv. Func. Mater. 16 (2006) 2324–2329.
[30] P.A. Vinodhini, G. Thandapani, V. Javachandran, A. Sukumaran, FTIR, XRD and DSC studies of nanochitosan, cellulose acetate and polyethylene glycol blend ultrafiltration membranes, Int. J. Biol. Macromol. 104 (2017) 1721–1729.
[31] W.G. Lee, D.H. Kim, W.C. Jeon, S.K. Kwak, S.J. Kang, S.W. Kang, Facile control of nanoporosity in cellulose acetate using nickel(II) nitrate additive and water pressure treatment for highly efficient battery gel separators, Sci. Rep. 7 (2017) 1287–1295.
[32] H. Song, B. Sun, T. Wang, S. Lu, L. Yang, B. Chen, X. Wang, X. Kong, Three-photon upconversion luminescence phenomenon for thegreen levels in Er3C/Yb3Ccodoped cubic nanocrystalline yttria, Solid St. Commun. 132 (2004) 409–413.
[33] L. Lyu, H. Cheong, X. Ai, W. Zhang, J. Li, H.H. Yang, J. Lin, B. Xing, Near-infrared light-mediated rare-earth nanocrystals: recent advances in improving photon conversion and alleviating the thermal effect, NPG Asia Mater. 10 (2018) 685–702.
[34] G. Chen, H. Qiu, P.N. Prasad, X. Chen, Upconversion nanoparticles: design, nanochemistry, and applications in theranostics, Chem. Rev. 114 (2014) 5161–5214.
[35] L. Mei, Y. Liu, C. Xia, Y. Zhou, Z. Zhang, Q. He, Polymer-drug nanoparticles combine doxorubicin carrier and heparin bioactivity functionalities for primary and metastatic cancer treatment, Mol. Pharm. 14 (2017) 513–522.
[36] L. Zhu, C. Wang, D.W. Pang, Z.L. Zhang, Controlled release of therapeutic agents with near-infrared laser for synergistic photochemotherapy toward cervical cancer, Anal. Chem. 91 (2019) 6555–6560.
[37] M. Dadsetan, K.E. Taylor, C. Yong, Z. Bajzer, L. Lu, Controlled release of doxorubicin from pH-responsive microgels, Acta Biomater. 9 (2013) 5438–5446.
[38] O. Kuchuk, A. Tuccitto, D. Citterio, V. Huber, C. Camisaschi, M. Milione, B. Vergani, A. Villa, M.R. Alison, S. Carradori, C.T. Supuran, L. Rivoltini, C. Castelli, V. Mazzaferro, pH regulators to target the tumor immune microenvironment in human hepatocellular carcinoma, Oncoimmunology 7 (2018) 1–14, e1445452.
[39] S. Rivankar, An overview of doxorubicin formulations in cancer therapy, Cancer Res. Ther. 10 (2014) 853–858.
[40] A.R. Chowdhuri, D. Laha, S. Pal, P. Karmakar, S.K. Sahu, One-pot synthesis of folic acid encapsulated upconversion nanoscale metal organic frameworks for targeting, imaging and pH responsive drug release, Dalton Trans. 45 (2016) 18120–18132.
[41] J. Zhao, H. Yang, J. Li, Y. Wang, X. Wang, Fabrication of pH-responsive PLGA (UCNPs/DOX) nanocapsules with upconversion luminescence for drug delivery, Sci. Rep. 7 (2017) 18014–18024.